

Article

CO₂ Adsorption Performance on Surface-Functionalized Activated Carbon Impregnated with Pyrrolidinium-Based Ionic Liquid

Syeda Saba Fatima ¹, Azry Borhan ^{2,*}, Muhammad Ayoub ¹ and Noraini Abd Ghani ³

¹ Department of Chemical Engineering, Universiti Teknologi PETRONAS, Bandar Seri Iskandar 32610, Perak, Malaysia

² HICoE, Centre of Biofuel and Biochemical Research, Institute of Self-Sustainable Building, Department of Chemical Engineering, Universiti Teknologi PETRONAS, Bandar Seri Iskandar 32610, Perak, Malaysia

³ Department of Fundamental and Applied Sciences, Universiti Teknologi PETRONAS, Bandar Seri Iskandar 32610, Perak, Malaysia

* Correspondence: azrybo@utp.edu.my

Abstract: The serious environmental issues associated with CO₂ emissions have triggered the search for energy efficient processes and CO₂ capture technologies to control the amount of gas released into the atmosphere. One of the suitable techniques is CO₂ adsorption using functionalized sorbents. In this study, a functionalized activated carbon (AC) material was developed via the wet impregnation technique. The AC was synthesized from a rubber seed shell (RSS) precursor using chemical activation and was later impregnated with different ratios of [bmpy][Tf₂N] ionic liquid (IL). The AC was successfully functionalized with IL as confirmed by FTIR and Raman spectroscopy analyses. Incorporation of IL resulted in a reduction in the surface area and total pore volume of the parent adsorbent. Bare AC showed the largest S_{BET} value of 683 m²/g, while AC functionalized with the maximum amount of IL showed 14 m²/g. A comparative analysis of CO₂ adsorption data revealed that CO₂ adsorption performance of AC is majorly affected by surface area and a pore-clogging effect. Temperature has a positive impact on the CO₂ adsorption capacity of functionalized AC due to better dispersion of IL at higher temperatures. The CO₂ adsorption capacity of AC (30) increased from 1.124 mmol/g at 25 °C to 1.714 mmol/g at 40 °C.

Keywords: CO₂ capture; activated carbon; functionalization; ionic liquid; biomass; wet impregnation



Citation: Fatima, S.S.; Borhan, A.; Ayoub, M.; Ghani, N.A. CO₂ Adsorption Performance on Surface-Functionalized Activated Carbon Impregnated with Pyrrolidinium-Based Ionic Liquid. *Processes* **2022**, *10*, 2372. <https://doi.org/10.3390/pr10112372>

Academic Editors: Jun Wei Lim and Worapon Kiatkittipong

Received: 15 October 2022

Accepted: 10 November 2022

Published: 12 November 2022

Publisher's Note: MDPI stays neutral with regard to jurisdictional claims in published maps and institutional affiliations.



Copyright: © 2022 by the authors. Licensee MDPI, Basel, Switzerland. This article is an open access article distributed under the terms and conditions of the Creative Commons Attribution (CC BY) license (<https://creativecommons.org/licenses/by/4.0/>).

1. Introduction

Over the years, a massive increase in greenhouse gas (GHG) emissions has led to the warming of the earth's atmosphere and these emissions are likely to increase further in future. The primary cause of GHG emissions is the rapid progress of modern civilization and industrial development [1]. Anthropogenic CO₂ is the main contributor to GHG emissions and is largely discharged from fossil fuel combustion from both vehicles and industries. Over 30 billion tons of CO₂ are released in the atmosphere every year [2]. This alarming increase of CO₂ in the atmosphere has already triggered climate issues, such as acid rain, melting of the ice caps and urban smog. Therefore, the need of the hour is to stabilize the level of CO₂ in the atmosphere to avoid irreversible and perpetual destruction of the atmosphere. This requires reducing the use of fossil fuels by using alternative fuel sources such as biofuels, promoting reforestation and using separation methods for CO₂ removal to reduce the daily release of the gas from prime sources, especially power plants and refineries [3].

Many separation techniques are available for post-combustion CO₂ capture, including absorption, membrane separation, cryogenic distillation, adsorption, chemical looping combustion and hydrate-based CO₂ capture [4]. Adsorption is a suitable separation method

because of its numerous advantages, including a wide range of solid adsorbents, high CO₂ adsorption capacity, easy regeneration and good selectivity at low concentrations [5,6]. Although many adsorbent materials have been explored for CO₂ capture [7–9], researchers are still trying to come up with new and advanced adsorbents and explore the adsorption kinetics and thermodynamics for better performing materials. Despite extensive research, adsorption is still far from large-scale applications due to technical and economic difficulties. Since the adsorption process itself is a costly process, development of cheaper solid adsorbents is required to make this method economically desirable. Biomass-derived adsorbents are especially important in this context. The most common precursors include agricultural waste, woody and non-woody biomass, industrial by-products and sludge. The first two categories are important because of their high carbon content and the low ash content of the resulting activated carbon (AC) [10]. Different fruit peels and fruit stones have been used to synthesize AC with high porosity, large surface area and good adsorption properties. These include banana peel [6], olive stone [11,12], coconut shell [13] and peanut shell [14]. Other waste materials used as raw materials for preparing porous AC include rice husk [15], bamboo [16], tea shell [8], tobacco [17] and eucalyptus wood [18]. Malaysia is a leading rubber-producing country after Thailand and Indonesia. According to the Department of Statistics Malaysia (DOSM), the stocks of rubber production were recorded at 296,328 tonnes in February 2020 [19]. This huge production rate also generates large quantities of solid waste laying around due to poor waste management. Rubber seed shell (RSS) is suitable as a precursor for the synthesis of AC due to its high carbon content, low cost and availability [7].

AC can be synthesized by either physical activation or chemical activation. The chemical activation method has the advantages of shorter activation time and lower temperature, and is generally preferred over the physical activation method [20]. Chemical activation involves the impregnation of the precursor with activating agents (such as KOH, NaOH, K₂CO₃, HNO₃ or ZnCl₂) and carbonization under inert or limited oxygen environment, followed by washing to remove impurities to obtain porous AC. Quan et al. (2019) [8] used tea seed shells to produce highly porous AC using KOH activation and reported a CO₂ adsorption capacity of 3.15 mmol/g at 25 °C and 1 bar. Plaza et al. (2012) [15] synthesized AC from spent coffee grounds using both physical activation and chemical activation methods. AC produced by physical activation showed higher selectivity for CO₂/N₂ and CO₂/He streams. Borhan et al. (2019) [7] developed microporous AC from RSS using KOH activation. A maximum surface area of 1129 m²/g and maximum CO₂ adsorption capacity of 54.3 mg/g at 25 °C and 1.25 bar were observed.

Although biomass-derived AC shows good CO₂ adsorption performance, it cannot compete with non-carbonaceous adsorbents, such as zeolites and metal organic frameworks (MOFs) [21]. Studies show that the performance of an adsorbent can be enhanced for CO₂ adsorption capacity, selectivity and the range of favorable adsorption conditions by treatment with suitable functional groups [22–26]. Surface functionalization introduces additional active sites and improves the CO₂ adsorption capacity. Surface functionalization can be performed by either grafting or impregnation methods. Grafted adsorbents show faster kinetics and improved thermal stability because of covalent bonding [27]. Unlike grafting, impregnation results in physical attachment of the functional groups to the surface of the adsorbent. The impregnated adsorbents are easily regenerated to their original adsorption capacity compared to the grafted ones [28]. Impregnation is usually preferred due to simpler experimental procedures and higher CO₂ adsorption capacity compared to grafting [4]. Researchers have used both functionalization techniques to prepare surface-functionalized solid adsorbents [29,30]. Amines or aminosilanes are the most common chemicals used for surface functionalization of solid adsorbents for CO₂ separation applications [24,31–36]. The reason for this is the high affinity of amino groups towards acidic gases like CO₂ and SO₂. Bezerra et al. (2011) [33] prepared monoethanolamine (MEA) impregnated AC and zeolite 13X. Prepared adsorbents showed a CO₂ adsorption capacity of 45 mg/g and 136 mg/g at 1 bar and 25 °C. It was observed

that the incorporation of amine groups improves the CO₂ adsorption capacity at high temperatures (70–90 °C) due to the contribution of chemisorption, whereas physisorption was found to be dominant at low temperatures (25–30 °C) [22]. Arenillas et al. (2005) [23] reported similar findings for Polyethyleneimine (PEI) impregnated fly ash with up to a 4.5% increase in CO₂ adsorption capacity at 75 °C over room temperature. On the other hand, commercial AC relying on physisorption alone showed lower CO₂ adsorption capacity at 75 °C. Sanz-Pérez et al. (2018) [30] prepared functionalized HMS mesoporous silica grafted with diethylenetriamine-trimethoxysilane (DT) and impregnated with PEI. Impregnated silica showed a higher CO₂ adsorption capacity (2.0 mmol/g) compared to grafted silica (1.8 mmol/g) at 45 °C and 1 bar. One major disadvantage with amine solvents is the leaching during the regeneration process that results in the formation of toxic byproducts and causes serious secondary pollution [37]. It also reduces the life of the functionalized adsorbent in repeated adsorption–desorption cycles. Ahmed et al. (2017) [38] reported a gradual decrease in the CO₂ adsorption capacity of PEI functionalized MCM-41 after six adsorption–desorption cycles due to the degradation of amino groups. Xu et al. (2002) [39] studied cyclic performance of MCM-41 impregnated with 50% PEI. Experimental findings showed a 5.3% decrease in the CO₂ adsorption capacity after seven cycles using pure CO₂. Similar findings were observed for pore expanded MCM-41 loaded with diethanolamine (DEA) [40]. Prepared adsorbent showed a reduction in the CO₂ adsorption capacity (3.3% lower than the initial value) after seven adsorption–desorption cycles due to slow loss of DEA, as confirmed by mass loss measurements using thermogravimetric analysis (TGA).

Ionic liquids (ILs) have emerged as a class of liquids with CO₂ solubility comparable to that of amines. However, their high prices and high viscosities are the main limitations in their practical application. Recent studies have focused on the use of ILs for surface functionalization, thus developing cost-effective adsorbent materials called the supporting ionic liquid phase (SILP). These hybrid adsorbents contain a thin layer of IL on the surface of a porous support. This arrangement provides a high gas–IL contact area and consequently higher mass transfer coefficients while reducing the amount of IL required, thus creating the critical economic benefit required for large-scale applications [41,42]. In this context, Ban et al. (2015) [43] investigated the effect of immobilized [C₄mim][Tf₂N] towards CO₂ selectivity of ZIF-8 and reported a five times higher CO₂/CH₄ and CO₂/N₂ selectivity in the low-pressure region (0–0.2 bar). The higher CO₂ uptakes result from the high solubility of CO₂ in [C₄mim][Tf₂N] and molecular sieving capacity of functionalized ZIF-8. Yusuf et al. (2017) [44] reported that coconut shell AC impregnated with 30 wt.% choline chloride adsorbed larger amounts of CO₂ compared to bare AC in a shorter time. Zhu et al. (2018) [29] studied the CO₂ adsorption performance of porous silica grafted and impregnated with three different ILs containing the same anion. The grafted silica showed faster diffusivity compared to impregnated silica, suggesting that more IL penetrated the inner pores and hindered the diffusion of CO₂ for the latter.

Despite a large number of research articles dealing with the use of different classes of ILs in functionalized adsorbents for CO₂ capture, there is still only fragmentary literature available on the use of biomass-derived AC for SILP and on the effect of confining ILs into micropores towards CO₂ capture. The selection of IL for surface functionalization is usually done based on the CO₂ solubility, viscosity, and thermal stability of the IL. Results from various studies have confirmed that the choice of an IL anion has the most direct effect on the CO₂ solubility, whereas the effect of an IL cation is less significant, but still noticeable [45]. Among various anions, [Tf₂N][−] shows the highest solubility of CO₂ due to larger number of fluoro groups [46]. Various studies have shown that ILs containing the [Tf₂N][−] anion paired with some imidazolium-based cations show good performance for CO₂ capture [45,47–50]. Unfortunately, the high cost of imidazolium based ILs limits their use. For this study, [bmpy][Tf₂N] IL with the [Tf₂N][−] anion and the pyrrolidinium substituted 1-butyl-1-methylpyrrolidinium bis(trifluoromethylsulfonyl)imide cation was selected for functionalization of RSS-based AC. Literature shows a higher solubility of CO₂ (3.3 mol-CO₂/kg-IL at 20 °C and 3.5 MPa) compared to H₂ (0.03 mol-H₂/kg-IL) in this

IL [51]. This opens the possibility of using a relatively cheaper IL for the functionalization of AC. This study aimed to prepare IL functionalized AC derived from RSS using six different ratios of IL, and to investigate the effect of IL loading and temperature on the CO₂ adsorption performance of the prepared adsorbent.

2. Materials and Methods

Rubber seeds were collected from Kampung Tersusun Tanah Hitam, Chemor, Perak 32100, Malaysia. The shells were separated after removing the inner white mass. The rubber seed shells (RSS) were then washed, dried, ground and sieved to obtain particles between 0.1 to 0.25 mm for further use.

Other chemicals including [bmpy][Tf₂N] (99.5%), K₂CO₃ (>99%) and methanol (99.8%) were purchased from Sigma Aldrich (M) Sdn. Bhd., Petaling Jaya, Selangor, Malaysia. Pure CO₂ (99.98%) for adsorption experiments was provided by Linde Malaysia Sdn. Bhd., Petaling Jaya, Selangor, Malaysia.

2.1. Synthesis of RSS Derived AC

A total of 30 g of ground RSS was activated by mixing it with 100 mL of 0.2 M aqueous K₂CO₃ solution. The mixture was left overnight to ensure that the K₂CO₃ had penetrated the RSS. The activated RSS was dried in an oven at 105 °C for 24 h, followed by carbonization in a tube furnace under N₂ atmosphere at 800 °C for 120 min. The nitrogen flow was set at 100 mL/min. AC was thus obtained was mixed with 0.01 M HCl to remove traces of salt and ash. The mixture was filtered and washed repetitively with distilled water to remove undissolved salt until a neutral pH was obtained. The AC was dried at 105 °C for 24 h. The dried sample was labelled as AC-fresh and stored in an airtight container. Ground and sieved RSS and prepared AC are shown in Figure 1.

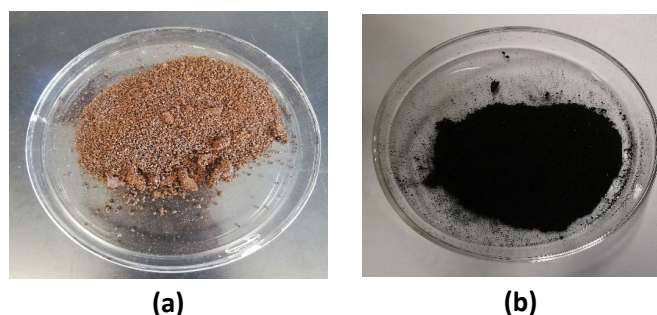


Figure 1. (a) Ground and sieved RSS with particle sizes of 0.1–0.25 mm dried at 105 °C (b) RSS AC activated by K₂CO₃ and carbonized at 800 °C for 180 min.

2.2. Preparation of Functionalized AC

RSS-derived AC was functionalized with six different concentrations of IL. Impregnation solution was prepared by mixing the desired amount of IL (10–60 wt.%) in 20 mL methanol. A fixed amount of AC was mixed with the impregnation solutions and stirred for 30 min at 350 rpm. The mixture was left overnight to ensure successful functionalization. Afterward, the AC samples were dried in an oven at 60 °C for 8 h to remove the solvent and stored in airtight bottles for further use. All functionalized AC samples were labelled as AC (x) with x representing the wt.% of the IL in the impregnation solution.

2.3. Characterization of Prepared Adsorbent

The AC samples were analyzed by a Field Emission Scanning Electron Microscope (FESEM) (Zeiss Supra 55 VP, Germany) using different magnification scales to study the structure and morphological properties before and after IL impregnation. The FESEM was equipped with an Energy Dispersive X-ray (EDX) analyzer to study the composition and distribution of the elements of interest. Surface functionalization was confirmed using

Fourier Transform Infrared Spectroscopy (FTIR) (Frontier 01, PerkinElmer, USA). IR spectra of fresh and functionalized AC were collected by the KBr pelleting method between the wavelength of 400 cm^{-1} to 4000 cm^{-1} . Thermal stability of the prepared AC samples was studied by TGA using a PerkinElmer, STA6000 instrument. The TGA profiles of all AC samples were obtained under N_2 flow for the temperature range of $30\text{--}750\text{ }^\circ\text{C}$ and a constant heating rate of $10\text{ }^\circ\text{C}/\text{min}$. The actual IL loading was quantified using individual TGA profiles. Surface properties of the AC before and after functionalization were estimated by performing surface area and porosity (SAP) analysis using a Brunauer–Emmett–Teller (BET) surface area analyzer (Micromeritics, Tristar 3020 Plus). The relevant surface properties, namely the BET specific surface area (S_{BET}), total pore volume (V_p), microporous surface area (S_{micro}), percentage of micropores and mesopores and the average pore diameter (n), were estimated from the N_2 adsorption isotherms obtained at 77 K . A Raman spectrometer (Horiba, Jobin Yvon HR) was used to examine the extent of the functionalization of the AC. The peaks appear between 200 to 2000 cm^{-1} . The spectrum of AC, like other carbon-based materials, is characterized by graphite (G) and disoriented (D) bands. The intensity ratio (I_D/I_G) was used to quantify the maturity of sp^2 hybridized carbon, which determines the extent of functionalization and increases with disorder in the structure.

2.4. CO_2 Adsorption Test

The adsorption performance of bare and functionalized AC for pure CO_2 (99.98%) was studied using the High Pressure Volumetric Analyzer (HPVA II). The experimental setup of the HPVA system is shown in Figure 2a. Each sample was weighed and placed into the sample holder. Before the adsorption experiment, the prepared sample was degassed under a vacuum for 4 h at $150\text{ }^\circ\text{C}$ to ensure a complete removal of impurities. Upon completion of degassing, the sample was cooled to room temperature and transferred to the analysis port. First, helium gas was introduced for free space volume measurement at the ambient and analysis temperatures. Purified helium was injected into the manifold. The gas was allowed to expand into the sample cell once pressure was equilibrated by opening valve (1) while all other valves were kept closed. The temperature and pressure readings were monitored throughout. The amount of helium dosed was obtained using Equation (1) and the free space volume was calculated using Equation (2).

$$n_D = \frac{P_A V_m}{T_A Z_A R} - \frac{P_B V_m}{T_B Z_B R} \quad (1)$$

$$V_{\text{AFS}} = V_s + V_{xL} + V_{xU} \quad (2)$$

Figure 2b shows that the upper stem was placed inside the temperature-controlled zone, and therefore its volume (V_{xU}) was assumed to be at the manifold temperature (T_B) after helium dosing. The lower stem volume (V_{xL}) was exposed to ambient temperature (i.e., 298 K). The free space volume at the analysis temperature (V_s) consisted of the volume of the sample cylinder and the stem volumes, was set to the targeted temperature. For free-space measurement at ambient temperature, V_s and V_{xL} were assumed to be at the same temperature as represented in Equation (3).

$$V_{sxL} = V_s + V_{xL} \quad (3)$$

The overall mass balance for calculating V_{sxL} is represented by Equation (4).

$$n_D + \frac{P_{s0} V_{xU}}{T_A Z_{xU0} R} + \frac{P_{s0} V_{sxL}}{T_{s0} Z_{s0} R} = \frac{P_{s1} V_{xU}}{T_B Z_{xU1} R} + \frac{P_{s1} V_{sxL}}{T_{s1} Z_{s1} R} \quad (4)$$

P_{s0} is assumed to be zero since the system was evacuated before the start of the experiment. The net mass balance after combining Equations (3) and (4) is presented in Equation (5).

$$n_D = \frac{P_{s1} V_{xU}}{T_B Z_{xU1} R} + \frac{P_{s1} V_{sxL}}{T_{s1} Z_{s1} R} \quad (5)$$

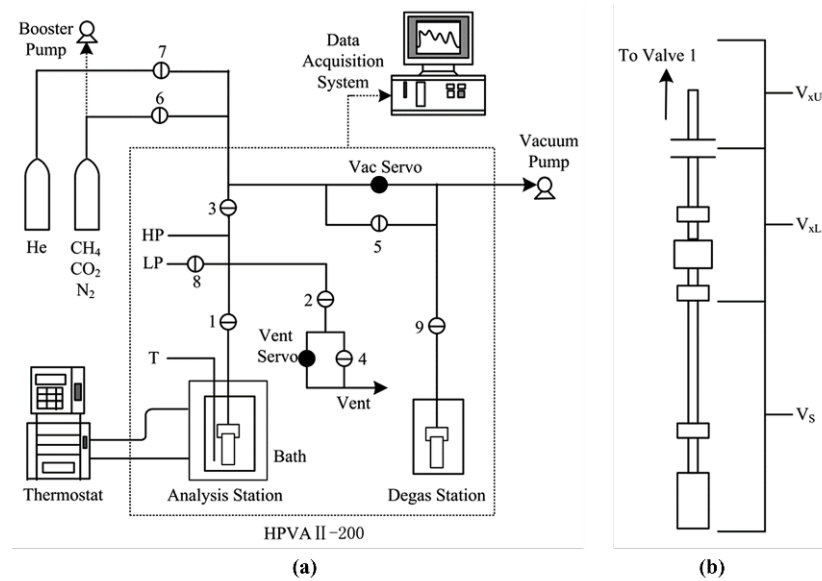


Figure 2. (a) Experimental set-up of HPVA equipment used for CO₂ adsorption study. HP, high pressure transducer; LP, low pressure transducer; T, temperature probe; (1), analysis port valve; (2) vent valve; (3) manifold valve; (4) external vent valve; (5) full vacuum valve; (6) inlet valve for CH₄/CO₂/N₂ gas; (7) inlet valve for He gas; (8) 1000 torr isolation valve; (9) degassing port valve. (b) Parts of HPVA system below valve 1 under different temperature zones [52].

Once V_{sxL} and n_D are known, free space volume is calculated using Equation (2). For free space measurement at the targeted temperature, V_s and V_{xL} were not at the same temperature. Therefore, V_s was estimated using the material balance in Equation (6) and later the free space volume was obtained from Equation (2).

$$n_D = \frac{P_{s1}V_{xU}}{T_B Z_{xU} R} + \frac{P_{s1}(V_{sxL} - V_s)}{T_{AM} Z_{xL1} R} + \frac{P_{s1}V_s}{T_{s1} Z_{s1} R} \quad (6)$$

After free space measurement, the sample cell was evacuated to remove the helium gas completely and the adsorbate (CO₂) was dosed for the adsorption test. The adsorbate was similarly expanded into the sample cell once the pressure was stable. After the adsorption test was complete, desorption was carried out by reducing the pressure in the sample cell at the same intervals. The adsorption study was conducted at 25 °C and 40 °C. The temperature was maintained by coupling the system with a Julabo recirculating water bath. The pressure and temperature data were recorded in a comprehensive data analysis package using Microsoft Excel macro (v.22.0.6) software. The compressibility factor was determined using NIST Reference Fluid Thermodynamic and Transport Properties incorporated in the software. The moles of the adsorbate (CO₂) dosed were calculated using Equation (7).

$$n_{Dosed} = \frac{P'_A V_m}{T'_A Z'_A R} - \frac{P'_B V_m}{T'_B Z'_B R} \quad (7)$$

The remaining amount of adsorbate (i.e., the amount not adsorbed) was calculated using Equation (8). Finally, the amount of adsorbate (CO₂) adsorbed by the sample was estimated by a simple mass balance shown in Equation (9). Each adsorption test was repeated twice. The experimental adsorption capacity is reported as mmol CO₂/g adsorbent.

$$n_{Nadsorb} = \frac{P_s}{R} \left(\frac{V_{sxL}}{Z_s T_s} + \frac{V_{xU}}{Z_{xU} T_{xU}} \right) \quad (8)$$

$$n_{Adsorb} = n_{dosed} - n_{Nadsorb} \quad (9)$$

3. Results and Discussion

Prepared AC samples were analyzed by various characterization techniques to study their structure and CO₂ adsorption performance. The effect of key variables, including IL loading and adsorption temperature on CO₂ adsorption performance, were studied. The details are presented in the following section.

3.1. FESEM and EDX Mapping

The surface chemistry of an adsorbent plays an important role in determining its adsorption properties. A porous surface indicates more active sites and yields higher CO₂ adsorption capacity. The structure and morphological properties of fresh functionalized AC were examined through FESEM under different magnification scales and the respective images are presented in Figure 3, which clearly shows the difference in the structure of AC before and after functionalization. Fresh AC has a highly porous surface with a combination of smaller and larger pores. This fine porosity of AC has resulted in high S_{BET} and V_p . On the contrary, functionalized AC has fewer surface pores due to the pore filling effect of the IL. This effect is more pronounced in AC samples impregnated with higher amounts of IL. At lower IL loading (10–20 wt.%), solvent molecules penetrate the narrow channels of AC, and surface porosity remains intact. As the IL loading is increased, inner pores start to fill up, which in turn reduces the available surface area. At very high IL loading (40–60 wt.%), a layer of bulk liquid is prominent on the surface, blocking most of the pores. This pore clogging and the presence of a thick liquid layer leads to a decrease in CO₂ adsorption capacity due to poor diffusion and low S_{BET} . Aside from examining the structure, the elemental composition of AC before and after functionalization was also analyzed using EDX mapping analysis. The elemental composition is presented in Table 1. Carbon and oxygen are the key elements with maximum composition present in all samples. Small amounts of potassium were also found due to the K₂CO₃ used for the chemical activation of the AC. The quantity of potassium is small and is attributed to the traces of salt left behind after washing. All functionalized AC samples have some quantities of fluorine and sulfur. The absence of both of these elements in the fresh AC confirms that their origin is from the IL and indicates the presence of IL functionalities in functionalized AC samples. The amount of both elements generally increases with increasing IL loading until saturated at 50 wt% loading. The maximum amounts of fluorine and sulfur are found in AC (50) as 12.97% and 3.72%, respectively.

Table 1. Elemental composition of RSS derived activated carbon (AC).

Elements		AC-Fresh	AC (10)	AC (20)	AC (30)	AC (40)	AC (50)	AC (60)
Carbon	Weight (%)	77.42	70.25	61.97	69.44	67.50	65.15	67.78
	Atomic (%)	84.33	78.49	73.60	78.61	76.37	74.58	76.90
Oxygen	Weight (%)	16.79	19.80	20.63	14.73	16.76	13.99	14.49
	Atomic (%)	13.77	16.61	18.39	12.52	14.23	12.02	12.34
Potassium	Weight (%)	5.79	4.91	11.58	4.37	3.33	2.58	2.91
	Atomic (%)	1.94	1.68	4.22	1.52	1.16	0.91	1.02
Fluorine	Weight (%)		3.84	3.89	8.51	10.20	12.97	11.82
	Atomic (%)		2.72	2.92	6.09	7.30	9.38	8.48
Sulfur	Weight (%)		1.20	1.93	2.74	2.22	3.72	3.00
	Atomic (%)		0.50	0.86	1.16	0.94	1.60	1.27

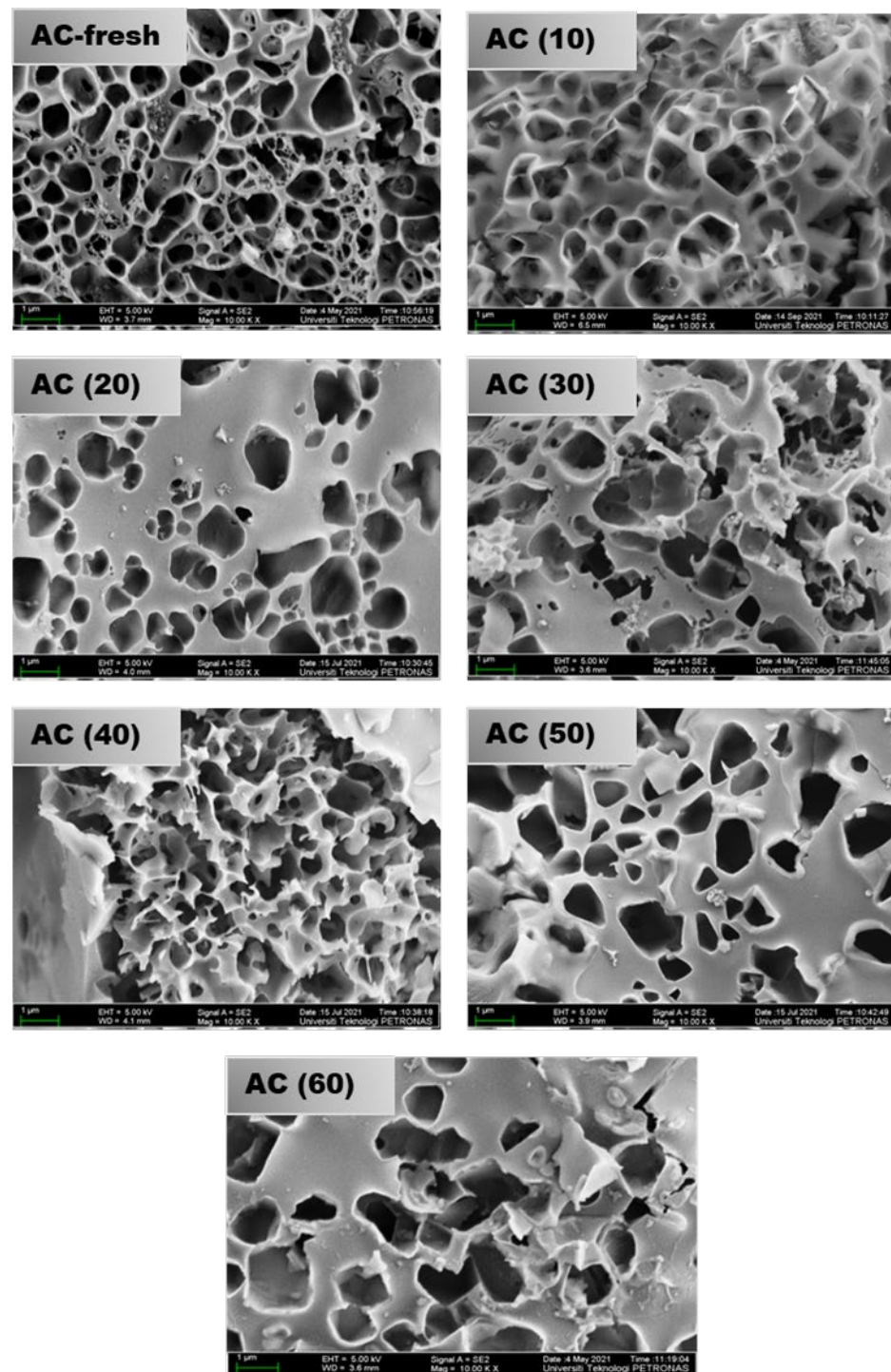


Figure 3. FESEM images of fresh activated carbon (AC) and functionalized with different concentrations of IL obtained at 1 µm (10,000× magnification scale).

Elemental mapping was also performed to study the spatial distribution of key elements. The relevant results are presented in Figure 4. Fresh AC (Figure 4a) has a homogeneous presence of carbon and oxygen as the building blocks of its structure. A small amount of potassium from the residual traces of K_2CO_3 is also uniformly scattered. Functionalized AC (Figure 4b) also shows a homogeneous presence of carbon, oxygen and potassium. In addition, significant amounts of fluorine and sulfur are present due to functionalization. Both elements are evenly distributed and confirm a homogeneous dispersion of IL in the form of a liquid layer of uniform thickness.

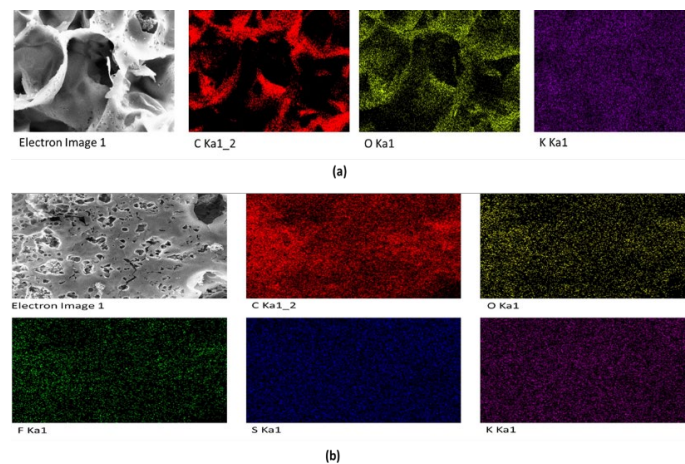


Figure 4. (a) EDX elemental mapping of fresh AC for C, O and K. (b) EDX elemental mapping of IL functionalized AC for C, O, F, S and K.

3.2. TGA

TGA measures variation in the weight of a sample with temperature and is used to estimate the thermal stability of the prepared adsorbent material. The TGA profiles of fresh and functionalized AC samples are presented in Figure 5. There are three regions of weight loss. The first stage accounts for changes in the mass of adsorbent below 200 °C and occurs due to the presence of surface bounded moisture. The second stage of weight loss, also called the rapid weight loss region, is from 200 °C to 600 °C. Major mass loss occurs during this stage due to the decomposition of tethered groups. The third stage of mass loss is above 600 °C. The weight loss in this region is small and usually occurs slowly due to thermal decomposition of the solid. The weight loss of fresh and functionalized AC samples in all three thermal stability regions is presented in Table 2. The weight loss during the first stage was less than 10% for all functionalized samples due to the hydrophobic nature of the IL and AC. The weight loss in the second stage (200–600 °C) is due to the decomposition of IL functionalities. The difference in the degradation temperature and the weight loss during the second stage indicates that each functionalized sample had a different amount of IL functional groups attached to the surface of AC. The weight changes in this stage are used to calculate the amount of IL loaded using Equation (10).

$$\gamma_{IL} = \frac{(\Delta wt\%_{imp} - \Delta wt\%_{raw})}{100MW_{IL}} \quad (10)$$

where γ_{IL} is the specific molar amount of IL impregnated on the support (mmol/g). $\Delta wt\%_{imp}$ and $\Delta wt\%_{raw}$ are the percentage mass loss during the rapid weight loss region for the functionalized and fresh AC, respectively. MW_{IL} is the molecular weight of the IL (422.41 g/mol).

Table 2. Thermal stability regions and respective weight loss for fresh and functionalized AC.

Thermal Stability Regions	AC-fresh	AC (10)	AC (20)	AC (30)	AC (40)	AC (50)	AC (60)
Moisture Evaporation Region (Below 200 °C)	9.08	9.69	8.46	6.06	1.88	4.94	1.78
Rapid Weight Loss Region (200–600 °C)	52.00	25.54	32.81	32.30	38.37	48.17	51.64
Decomposition Region (Above 700 °C)	36.31	6.76	11.62	9.36	14	14.76	28.87

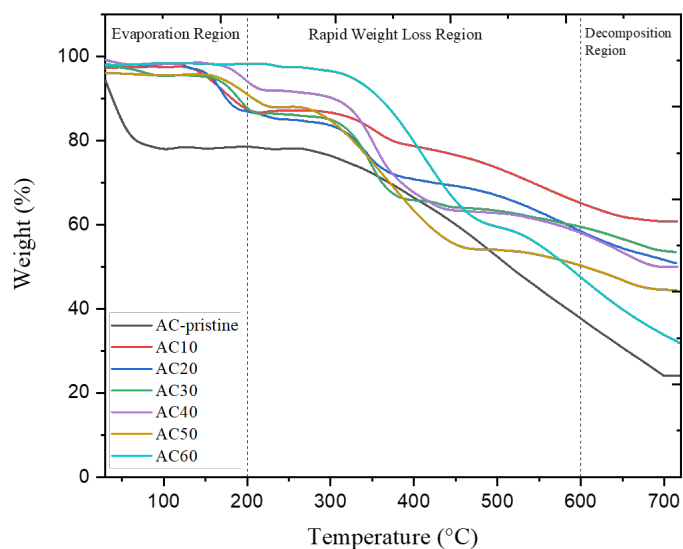


Figure 5. TGA profiles for fresh and functionalized AC under N₂ flow.

Weight loss in the third stage is associated with the decomposition of the graphite structure of the AC. Weight loss in the final stage for fresh AC was 36.3%, which is higher than functionalized AC. The lower relative stability of fresh AC at high temperatures is due to numerous surface defects in its structure, which accelerate combustion of the graphite network. Overall, the incorporation of IL improved the thermal stability of the AC. Similar findings were presented by Lemus et al. (2011) for imidazolium-based IL impregnated on three different supports [42].

3.3. FTIR Analysis

Surface functionalization improves the surface capturing properties of an adsorbent and results in higher uptake of the adsorbate due to additional active sites containing affinity groups. The study of surface groups was performed using FTIR analysis. IR spectra of fresh AC and AC functionalized with different amounts of IL are presented in Figure 6. A comparison between these spectra shows the presence of additional peaks in the functionalized AC samples. The additional peaks in functionalized samples resulted from the interactions between the IL functional groups and the porous support. The characteristic peaks are identified using the available literature on FTIR spectroscopy analysis and are similar to the findings reported previously [53].

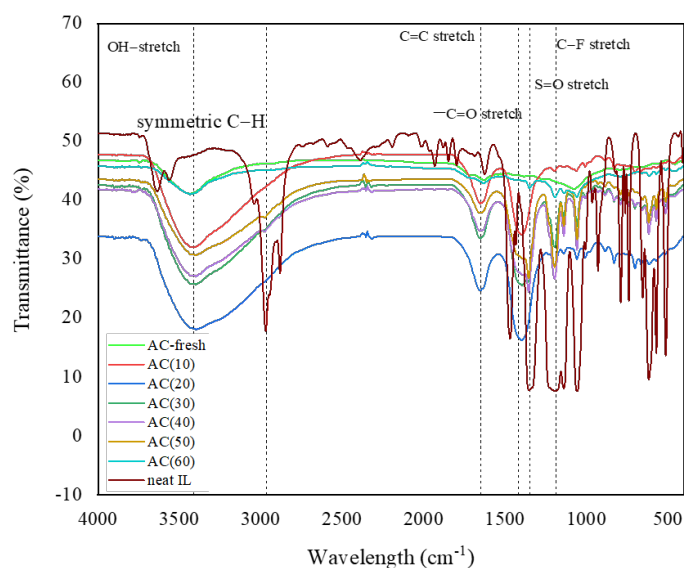


Figure 6. FTIR spectra of fresh and functionalized AC.

A broad peak observed for fresh AC at 3434 cm^{-1} is assigned to OH-stretching vibrations caused by the presence of surface hydroxyl groups. Similar peaks are observed in functionalized AC samples at 3432 cm^{-1} , 3399 cm^{-1} , 3400 cm^{-1} , 3401 cm^{-1} , 3400 cm^{-1} and 3432 cm^{-1} with reduced intensity. Because of the hydrophobic nature of IL, functionalized samples retain smaller amounts of moisture, hence a lower intensity of the hydroxyl group peak. The neat IL spectrum has distinguished peaks between 2900 cm^{-1} and 2500 cm^{-1} because of the C-H stretching of alkanes. Alkenes form the backbone of carbon structure and are indicated by the presence of the C=C stretching at 1600 cm^{-1} in the fresh AC spectrum. The same peak appears in the impregnated samples at 1650 cm^{-1} , 1650 cm^{-1} , 1648 cm^{-1} , 1653 cm^{-1} , 1648 cm^{-1} and 1631 cm^{-1} , which confirms that the structure of the AC remains intact after the incorporation of IL. For functionalized AC samples, sharp peaks are observed near 1468 cm^{-1} and 1352 cm^{-1} , indicating the presence of the S=O stretching of the sulfonyl group, while the smaller peaks between $1100\text{--}1000\text{ cm}^{-1}$ show the presence of the fluoro group. The presence of both functional groups is confirmed from the neat IL spectrum and are originated from the $[\text{Tf}_2\text{N}]^-$ anion of the IL. The intensity of these peaks is higher in AC samples impregnated with a higher dosage of IL, which indicates a higher level of surface functionalization in these samples.

3.4. SAP Analysis

The shape of the adsorption isotherm provides useful information regarding the adsorption process. Nitrogen adsorption isotherms of fresh and functionalized AC obtained at 77 K are presented in Figure 7. According to the classification of the International Union of Pure and Applied Chemistry (IUPAC), all isotherms are identified as type I, representing microporous solids [54]. The N_2 uptake increases gradually in the region of low P/P_0 , followed by a plateau until $P/P_0 = 0.5$. Higher uptake is observed in the high-pressure region. These findings agree with those reported previously since physisorption is favorable under high pressure and low temperatures. The N_2 adsorption capacity is reduced for functionalized AC with increasing IL loading. After incorporating IL, surface active sites are covered with IL functionalities. N_2 does not interact with IL functionalities; therefore, less surface active sites are available for N_2 to be adsorbed and the adsorption capacity of AC is reduced. This effect becomes pronounced with increasing IL concentration until surface saturation is achieved. For the RSS AC prepared in this study, surface saturation was observed at an IL concentration of 60 wt.%, where negligible pore volume resulted in no N_2 adsorbed on the surface. Since N_2 is non-reactive, the lower N_2 uptake for functionalized samples is consistent with consistently low S_{BET} .

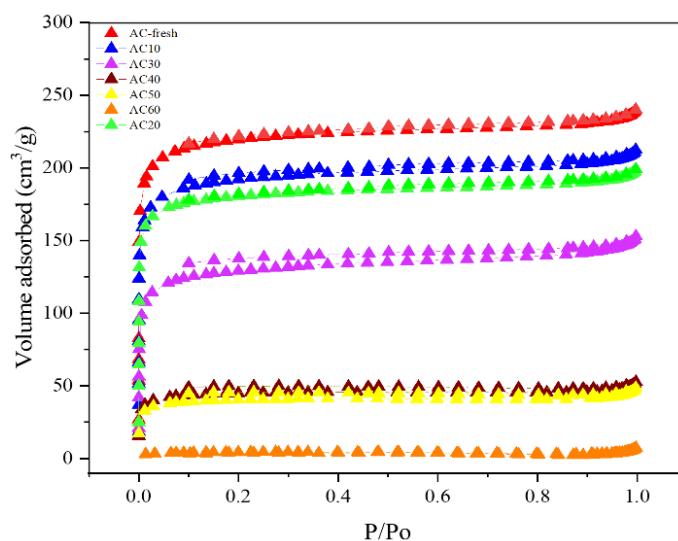


Figure 7. N_2 adsorption–desorption isotherm of fresh AC and functionalized with different amounts of IL at 77 K.

Surface properties play a significant role in estimating the adsorption capacity of an adsorbent. The relevant surface properties of fresh and functionalized AC were estimated by BET analysis and are presented in Table 3. CO₂ is adsorbed on fresh AC by only a physical attachment to the surface. Therefore, a porous surface is desirable because it provides more surface-active sites. The high porosity of fresh AC has resulted in high S_{BET} and V_p of 683 m²/g and 0.37 cm³/g, respectively. Functionalized AC shows a reduction in both S_{BET} and V_p with higher IL loading. At lower IL loading (10–20 wt.%), the reduction in S_{BET} is small. This shows that IL has penetrated the inner pores rather than sitting on the surface as a bulk liquid. However, as the concentration of the IL in the impregnation solution is increased above 30 wt.%, the inner pores of the AC are filled and a liquid layer covers most of the surface porosity. As a result, a very rapid decrease in the surface area is observed at higher IL loading. These surface area values are derived from micropores, which is evident from the high values of S_{micro} for all samples. AC (60) with maximum IL loading only has a surface area of 14 m²/g and negligible pore volume. A massive reduction of V_p from 0.07 cm³/g to merely 0.01 cm³/g for an increase of IL loading from 50 to 60 wt.% indicates surface saturation. Values of n are consistent and did not change significantly after functionalization.

Table 3. Surface properties of fresh and functionalized activated carbon.

Sample	Specific Surface Area (S_{BET})	T-Plot Micropore Area (S_{micro})	External Surface Area (S_{ext})	Total Pore Volume (V_p)	Average Pore Diameter (D)	Percent Micropores
	(m ² /g)	(m ² /g)	(m ² /g)	(cm ³ /g)	nm	(%)
AC-fresh	683	579	104	0.37	2.16	79.6
AC (10)	599	496	103	0.33	2.18	77.2
AC (20)	559	478	81	0.31	2.18	79.7
AC (30)	404	319	86	0.23	2.31	69.5
AC (40)	140	116	23	0.08	2.27	74.7
AC (50)	126	103	23	0.07	2.31	72.2
AC (60)	14	7	7	0.01	2.73	37.6

3.5. Raman Spectroscopy Analysis

Raman spectroscopy is widely used for the characterization of carbonaceous adsorbents to confirm the heterogeneous structure of microporous carbon. Raman spectra of fresh AC and functionalized AC samples with the highest CO₂ adsorption capacity (AC 30) are shown in Figure 8. For investigation of the structural properties of carbon, disoriented (D) band at 1380 cm⁻¹ and graphite (G) band at 1590 cm⁻¹ are important. The D-band is attributed to the defects of highly ordered sp³ carbon and aromatics with less than six rings, whereas the G-band represents the vibrations in the graphite structure due to ordered sp² carbon.

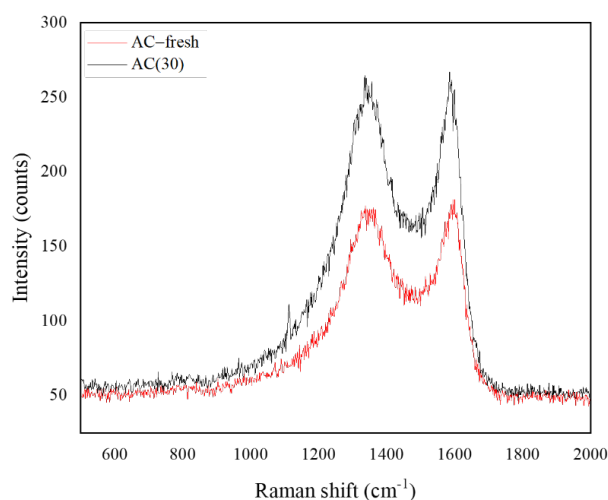


Figure 8. Raman spectra of fresh AC and functionalized AC (30).

The degree of functionalization is estimated using an I_D/I_G ratio. The value for fresh and functionalized AC is 0.918 and 0.967, respectively. A higher I_D/I_G ratio for functionalized AC indicates a change in symmetry. The interactions between the IL functional groups and carbon structure create a strain that creates a disorder in the structure and a change in symmetry from sp^2 to sp^3 carbon.

3.6. CO₂ Adsorption Study

The screening of adsorption performance was performed at 25 °C and 1 bar. Figure 9 depicts the CO₂ adsorption capacity of fresh and functionalized AC samples. Esteves et al. (2008) demonstrated that 25 °C is the ideal temperature for CO₂ adsorption because of the exothermic nature of physisorption that takes place for most of the physical adsorbents like AC [55]. Moreover, the selected conditions often reported in the literature are 0–1 bar pressure and 25 °C temperature. Therefore, the selected temperature allows for an easy comparison with earlier findings. Overall, the CO₂ adsorption capacity for functionalized AC increases with IL loading until reaching a maximum value at 30 wt.% IL loading. Afterwards, the CO₂ adsorption capacity remains nearly the same for the last three samples, indicating surface saturation. The CO₂ adsorption capacity measured at 25 °C is in the following order: AC-fresh (2.165 mmol/g) > AC (30) (1.124 mmol/g) > AC (20) (1.055 mmol/g) > AC (10) (0.758 mmol/g) > AC (40) (0.546 mmol/g) > AC (50) (0.533 mmol/g) > AC (60) (0.421 mmol/g). A similar trend is seen for CO₂ adsorption obtained at 40 °C. It is observed that S_{BET} has the most significant effect on the CO₂ adsorption capacity. The S_{BET} of the samples followed the order: AC-fresh (683.4 m²/g) > AC (10) (599 m²/g) > AC (20) (559 m²/g) > AC (30) (404 m²/g) > AC (40) (140 m²/g) > AC (50) (126 m²/g) > AC (60) (14 m²/g). As S_{BET} is reduced with increasing IL loading, fewer active sites are available, leading to lower adsorption of CO₂. The influence of the surface area is crucial in functionalized samples with higher IL loading. For IL loading (10–30 wt.%), the CO₂ adsorption capacity increases despite a reduction in the surface area, as is evident from a higher CO₂ adsorption capacity for AC (30) compared to AC (20) and AC (10). This indicates that other factors are affecting CO₂ adsorption. Besides surface area, IL loading also affects the CO₂ adsorption capacity of AC. For functionalized AC, CO₂ is adsorbed by a combination of chemisorption by IL functionalities and physisorption by the support.

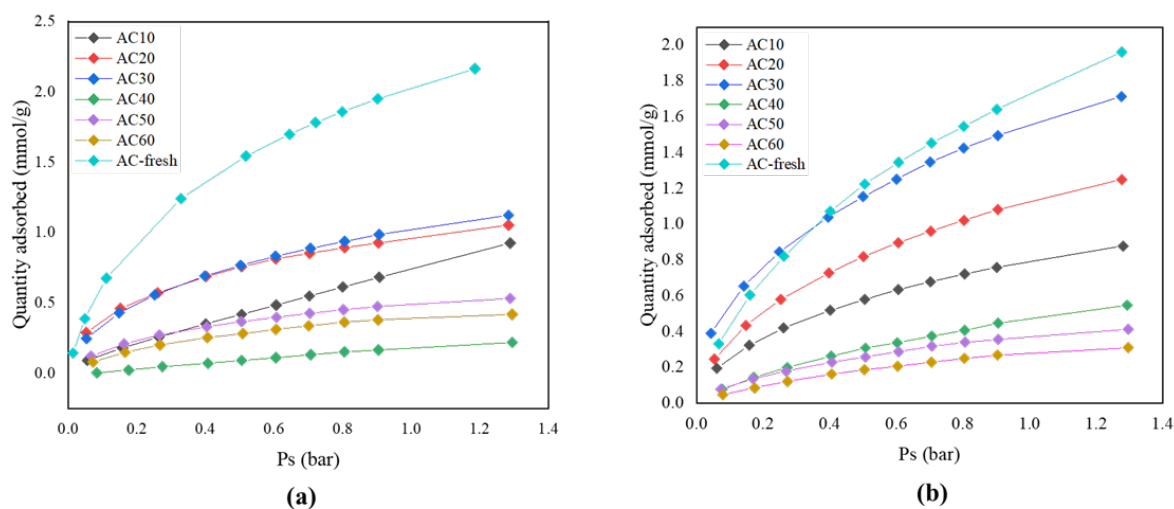


Figure 9. CO₂ adsorption capacity of fresh and functionalized AC obtained at (a) 25 °C and (b) 40 °C.

The effect of pressure on CO₂ adsorption is studied where higher adsorption takes place at higher pressure. Higher pressure pushes the CO₂ molecules into the pores. The percentage of CO₂ uptake of AC samples at both adsorption temperatures is presented in Figure 10. Fresh AC showed the highest uptake of 9.52 wt.% at 25 °C and 8.63 wt.% at

40 °C and 1.3 bar, whereas functionalized AC (30) showed the highest uptake of 4.748 wt.% at 25 °C and 7.54 wt.% at 40 °C and 1.3 bar.

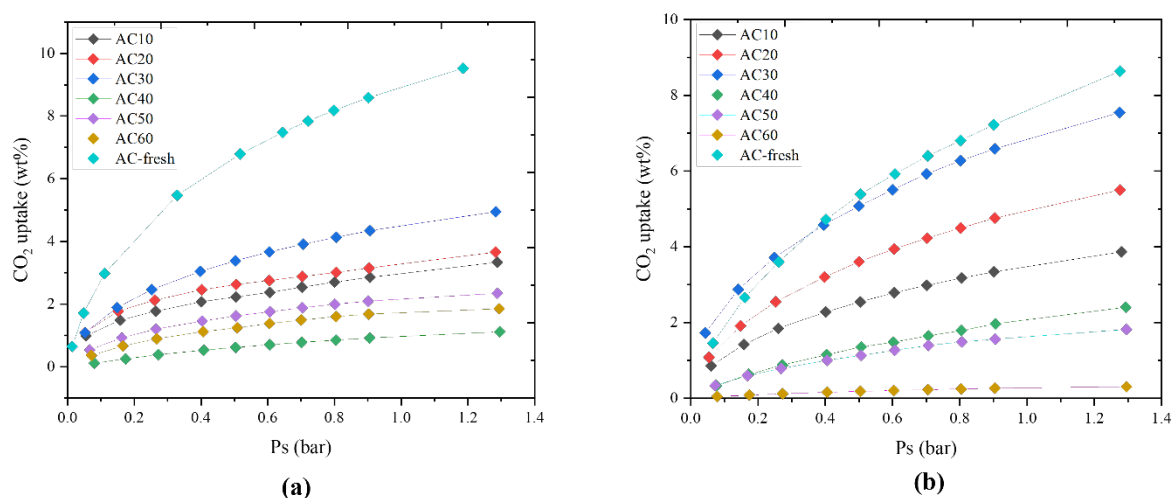


Figure 10. Percentage CO₂ uptake for fresh and functionalized AC obtained at (a) 25 °C and (b) 40 °C.

3.7. Effect of IL Loading

A reduction in the surface area and pore volume is observed with increasing IL concentration in the impregnation solution. The distribution of V_p with IL loading for each AC sample is presented in Figure 11. At IL loading (10–30 wt.%), IL penetrates the inner pores and there is a small decrease in V_p and S_{BET} values, as seen in Table 3. As the IL concentration is increased, the pore-clogging effect becomes prominent. For IL concentrations above 30 wt.%, inner pores are filled, and surface-active sites are reduced. There is a sharp decrease in pore volume at higher IL loadings (40–60 wt.%). AC (60) has a negligible pore volume, indicating the limitation of the amount of IL that can be impregnated.

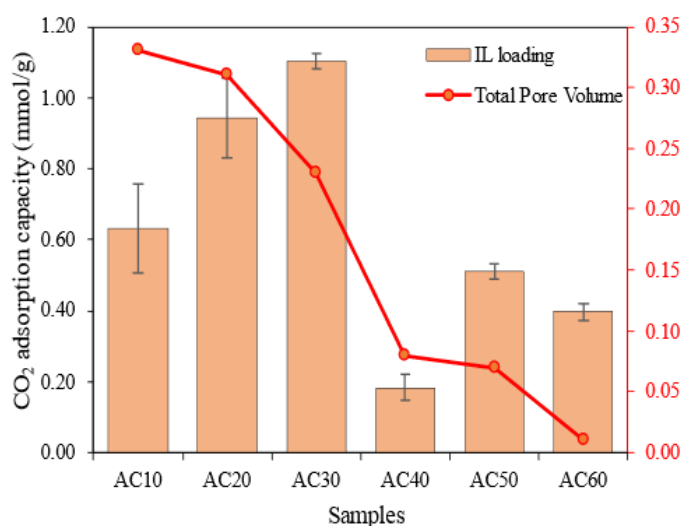


Figure 11. CO₂ adsorption capacity at 1 bar and 25 °C and total pore volume of AC functionalized with different amounts of IL.

The influence of IL loading on the CO₂ adsorption capacity was observed to identify the optimum IL loading with the best adsorption performance. The CO₂ adsorption capacity first increased for IL loading (10–30 wt.%) despite a reduction in the pore volume. AC (30) shows the highest CO₂ adsorption capacity of 1.124 mmol/g. For higher IL loadings (40–60 wt.%), the CO₂ adsorption capacity was reduced due to pore-clogging effect and

poor diffusion due to the active phase layer of the IL. The interaction between the IL functional groups and CO₂ is much stronger at lower IL loading and there is significant contribution of physisorption by the support. CO₂ molecules have stronger interactions with an anion of IL. Due to the larger size of the [Tf₂N][−] anion, maximum surface coverage was achieved at much lower loading. Afterward, IL molecules started depositing in a multilayer formation and increased the thickness of the active phase layer of the IL. At a higher IL loading (>30 wt%), the surface area was reduced and the contribution of physisorption by the support was minimal. Furthermore, a bulkier liquid layer makes the diffusion of CO₂ molecules difficult. Consequently, lower CO₂ adsorption capacity was observed at higher IL loadings. Overall, AC impregnated with 30 wt% IL showed the best performance among other functionalized samples.

3.8. Effect of Adsorption Temperature

The CO₂ adsorption capacity of all samples was tested at 25 °C and 40 °C, and the results are presented in Figure 12. The temperature had a pronounced effect on CO₂ adsorption capacity. For fresh AC, the CO₂ adsorption capacity was reduced from 2.16 mmol/g at 25 °C to 1.96 mmol/g at 40 °C. CO₂ was adsorbed on fresh AC by physisorption involving weak van der Waals forces. This interaction is favorable at low temperatures. At high temperatures, the CO₂ molecules move faster and the surface adsorption energy is increased, leading to desorption. Ammendola et al. (2017) reported that at high temperatures, the adsorbate molecules adsorbed on the surface gain sufficient energy and can easily escape the surface and diffuse back to the gaseous phase [56]. Tamilarasan and Ramaprabhu (2012) also reported similar findings and ascribed them to the kinetic energy of adsorbate molecules [57]. At low adsorption temperatures, CO₂ molecules interact with the surface and are adsorbed by a multilayer formation. However, at elevated adsorption temperatures, CO₂ molecules have a much higher velocity to overcome the weak forces of interaction and eventually escape from the pores of the AC. Therefore, lower CO₂ adsorption capacity is observed for fresh AC at 40 °C than at 25 °C.

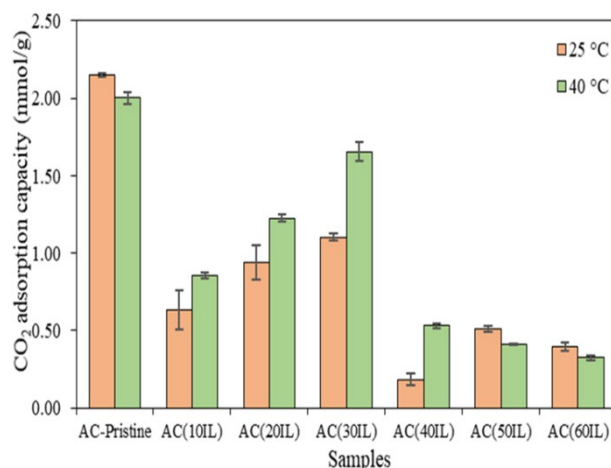


Figure 12. Effect of adsorption temperature on the CO₂ adsorption capacity.

For IL functionalized AC under dilute impregnation concentrations, the difference in the CO₂ adsorption capacity with respect to the fresh AC was reduced as the temperature was increased. High temperature has a favorable effect on the dispersion of IL in the pores of AC. This implies that as the temperature rises, a better distribution of IL on the surface of AC (due to reduced surface tension of IL) makes it easier for the CO₂ molecules to reach the inner active sites. Hence, it can be said that CO₂ adsorption for IL functionalized AC is more favorable at higher temperatures. For AC (30), a higher amount of CO₂ was adsorbed at 40 °C compared to 25 °C. Similar findings were reported for amine impregnated fly ash, where the CO₂ adsorption capacity increased at high temperatures [24,52]. Zhang et al. (2019) [58] prepared amine-functionalized SBA-15 and observed a high CO₂ adsorption

capacity at high temperatures due to higher reactivity of amine functionalities. Erto et al. (2015) [53] used two ILs for surface functionalization of AC and reported that the IL functionalized AC showed comparable CO₂ adsorption capacity as the raw AC at 80 °C despite showing a poor performance at room temperature. This phenomenon is attributed to a complex effect of temperature on the dispersion of IL. Although functionalized AC did not adsorb a high amount of CO₂ at 25 °C compared to fresh AC, it performed effectively at 40 °C. Based on this observation, we can expect a much higher CO₂ adsorption capacity for AC (30) at higher temperatures (70–120 °C).

3.9. Comparison with Previous Studies

The CO₂ adsorption performance of the prepared AC samples was compared with other biomass materials reported in literature. A summary of this comparison is presented in Table 4. RSS-derived AC has noticeably higher CO₂ adsorption capacity compared to some other biomass precursors including rice husk, palm kernels and bagasse pith. K₂CO₃ performs better than KOH for the same precursor (RSS) as evidenced by a higher CO₂ adsorption capacity for the former. The applicability of RSS for the development of AC is practical to replace traditional non-carbonaceous adsorbents like zeolites and silica. It is also a potential mechanism for solid waste management by utilizing agricultural waste.

Table 4. A comparison of CO₂ adsorption performance of various adsorbents.

Adsorbent	Functionalization Method	Chemicals	CO ₂ Adsorption Capacity at 25 °C (mmol/g)	Ref.
RSS AC	wet impregnation	K ₂ CO ₃	2.160	This study
RSS AC	wet impregnation	KOH	1.231	[7]
Rice husk	wet impregnation	ZnCl ₂	1.330	[15]
Bagasse pith	wet impregnation	ZnCl ₂	1.747	[59]
Palm kernel shell	physical activation	CO ₂	1.660	[60]
RSS AC	wet impregnation	[bmpy][Tf ₂ N]	1.124	This study
Palm shell AC	wet impregnation	PEI	0.759	[34]
SBA-15	wet impregnation	[bmim][BF ₄]	0.816	[61]
AC Norit CGP Super	wet impregnation	DETA	1.760	[22]
SBA-15	wet impregnation	[bmim][Ac]	0.926	[62]
SiO ₂	wet impregnation	[Emim][HSO ₄]	1.095	[63]
SiO ₂	grafting	[P8883][TFSI]	0.99	[29]
MCM-41	water-aided grafting	[(MeO) ₃ Sipmim][Cl]	1.48	[64]

The AC (30) prepared in this study performed better than many functionalized adsorbents including silica, zeolites and AC. The obtained CO₂ adsorption capacity was also higher than KOH-activated RSS and some other biomass precursors. The CO₂ adsorption capacity obtained for AC (30) in this study was better compared to other functionalized adsorbents. The [Tf₂N] anion performed better compared to [BF₄][−], [Cl][−] and [HSO₄][−] anions, as evidenced by a higher CO₂ adsorption capacity.

4. Conclusions

In this study, synthesis of surface-functionalized RSS-derived AC impregnated with [bmpy][Tf₂N], its detailed characterization and the CO₂ adsorption study were carried out. The synthesis of this adsorbent material not only aids in reducing the rising amount of CO₂, but also resolves the issue of land space covered by the selected biomass waste.

- FTIR and BET analyses of fresh and functionalized AC confirm successful functionalization with the selected IL. BET analysis shows that both S_{BET} and V_p are reduced with increasing IL concentration. The reduction of both surface properties is prominent at higher IL loading (40–60 wt%).
- The N₂ adsorption isotherm analysis shows type I isotherms for fresh and functionalized AC and suggests the properties of a microporous material.

- Raman spectroscopy confirms that the structure of AC is unharmed by the incorporation of IL. The improved thermal stability of the functionalized adsorbents compared to the fresh AC is confirmed through TGA.
- The CO₂ adsorption occurs by physisorption for fresh AC and is mainly affected by available surface area. The CO₂ adsorption capacity of functionalized AC is affected by IL loading and adsorption temperature. The CO₂ adsorption capacity initially increases with IL loading up to 30 wt.% and reduces afterward due to low surface area and resultant pore obstruction.
- The performance of functionalized AC is improved at higher adsorption temperature due to a better dispersion of IL.

Author Contributions: Conceptualization, A.B.; methodology, A.B., S.S.F. and M.A.; validation, A.B., M.A. and N.A.G.; formal analysis, A.B. and S.S.F.; investigation, S.S.F.; resources, A.B. and M.A.; data curation, S.S.F.; writing—original draft preparation, S.S.F.; writing—review and editing, A.B., M.A. and N.A.G.; supervision, A.B., M.A. and N.A.G.; funding acquisition, A.B. All authors have read and agreed to the published version of the manuscript.

Funding: This research work is funded by the Yayasan Universiti Teknologi PETRONAS, Malaysia, grant number (YUTP-FRG 015LC0-068).

Data Availability Statement: Original high-resolution images of FESEM and EDX analysis presented in Figures 3 and 4 are provided as supplementary information.

Acknowledgments: The authors graciously thank the HICoE, Centre of Biofuel and Biochemical Research (CBBR) and Institute of Self-Sustainable Building Universiti Teknologi PETRONAS (UTP) Malaysia for providing technical and financial assistance.

Conflicts of Interest: The authors declare no conflict of interest.

Nomenclature

n_D	moles of helium dosed into the sample cell (mol)
n_{Dosed}	moles of adsorbate dosed into the sample cell (mol)
$n_{Nadsorb}$	moles of adsorbate remaining in the sample cell (mol)
n_{adsorb}	moles of adsorbate adsorbed by the sample (mol)
P_A, P_B	pressure of the manifold before and after dosing (bar)
P_{s0}, P_{s1}	pressure of sample cell before and after dosing Helium (bar)
P'_A, P'_B	pressure of sample cell before and after dosing adsorbate (bar)
P_s	pressure of sample cell for adsorption (bar)
T_{AM}	ambient temperature (298 K)
T_A, T_B	temperature of the manifold before and after dosing (K)
T_{s0}, T_{s1}	temperature of sample before and after dosing Helium (K)
T'_A, T'_B	temperature of sample cell before and after dosing adsorbate (K)
T_s	temperature of sample cell for adsorption (K)
T_{xU}	manifold temperature (K)
Z_A	gas compressibility of helium at T_A and P_A
Z_B	gas compressibility of helium at T_B and P_B
Z_{s0}, Z_{s1}	gas compressibility at (T_{s0}, P_{s0}) and (T_{s1}, P_{s1}) respectively
Z_{xU0}, Z_{xU1}	gas compressibility at (T_A, P_{s0}) and (T_B, P_{s1}) respectively
Z_{xL0}, Z_{xL1}	gas compressibility at (T_{AM}, P_{s0}) and (T_{AM}, P_{s1}) respectively
Z'_A, Z'_B	gas compressibility at (T'_A, P'_A) and (T'_B, P'_B) respectively
Z_{xU}	gas compressibility at (T_{xU}, P_s)
R	universal gas constant $(83.14 \text{ cm}^3 \cdot \text{bar} \cdot \text{mol}^{-1} \cdot \text{K}^{-1})$
V_m	LP manifold volume (43.9311 cm^3)
V_{AFS}	free space volume at ambient temperature (cm^3)
V_{sxL}	manifold volume outside the temperature-controlled zone (cm^3)
V_s	free space volume at analysis temperature (cm^3)
V_{xL}	lower stem volume (cm^3)
V_{xU}	upper stem volume (3.5 cm^3)

References

1. Sher, F.; Iqbal, S.Z.; Albazzaz, S.; Ali, U.; Mortari, D.A.; Rashid, T. Development of biomass derived highly porous fast adsorbents for post-combustion CO₂ capture. *Fuel* **2020**, *282*, 118506. [CrossRef]
2. Li, B.; Duan, Y.; Luebke, D.; Morreale, B. Advances in CO₂ capture technology: A patent review. *Appl. Energy* **2013**, *102*, 1439–1447. [CrossRef]
3. Leung, D.Y.C.; Caramanna, G.; Maroto-Valer, M.M. An overview of current status of carbon dioxide capture and storage technologies. *Renew. Sustain. Energy Rev.* **2014**, *39*, 426–443. [CrossRef]
4. Fatima, S.S.; Borhan, A.; Ayoub, M.; Ghani, N.A. Development and progress of functionalized silica-based adsorbents for CO₂ capture. *J. Mol. Liq.* **2021**, *338*, 116913. [CrossRef]
5. Borhan, A.; Hoong, P.K.; Taha, M.F. Biosorption of heavy metal ions, oil and grease from industrial waste water by banana peel. *Appl. Mech. Mater.* **2014**, *625*, 749–752. [CrossRef]
6. Borhan, A.; Thangamuthu, S.; Taha, M.F.; Ramdan, A.N. Development of activated carbon derived from banana peel for CO₂ removal. In Proceedings of the AIP Conference Proceedings 2015, Negeri Sembilan, Malaysia, 24–26 February 2015.
7. Borhan, A.; Yusup, S.; Lim, J.W.; Show, P.L. Characterization and modelling studies of activated carbon produced from rubber-seed shell using KOH for CO₂ adsorption. *Processes* **2019**, *7*, 855. [CrossRef]
8. Quan, C.; Jia, X.; Gao, N. Nitrogen-doping activated biomass carbon from tea seed shell for CO₂ capture and supercapacitor. *Int. J. Energy Res.* **2019**, *44*, 1218–1232. [CrossRef]
9. Kumar, K.; Kumar, A. Enhanced CO₂ adsorption and separation in ionic-liquid-impregnated mesoporous silica MCM-41: A molecular simulation study. *J. Phys. Chem. C* **2018**, *122*, 8216–8227. [CrossRef]
10. Ao, W.; Fu, J.; Mao, X.; Kang, Q.; Ran, C.; Liu, Y.; Zhang, H.; Gao, Z.; Li, J.; Liu, G.; et al. Microwave assisted preparation of activated carbon from biomass: A review. *Renew. Sustain. Energy Rev.* **2018**, *92*, 958–979. [CrossRef]
11. Hazzaa, R.; Hussein, M. Adsorption of cationic dye from aqueous solution onto activated carbon prepared from olive stones. *Environ. Technol. Innov.* **2015**, *4*, 36–51. [CrossRef]
12. Yakout, S.M.; Sharaf El-Deen, G. Characterization of activated carbon prepared by phosphoric acid activation of olive stones. *Arab. J. Chem.* **2016**, *9*, 1155–1162. [CrossRef]
13. Chen, J.; Yang, J.; Hu, G.; Hu, X.; Li, Z.; Shen, S.; Radosz, M.; Fan, M. Enhanced CO₂ capture capacity of nitrogen-doped biomass-derived porous carbons. *ACS Sustain. Chem. Eng.* **2016**, *4*, 1439–1445. [CrossRef]
14. Deng, S.; Hu, B.; Chen, T.; Wang, B.; Huang, J.; Wang, Y.; Yu, G. Activated carbons prepared from peanut shell and sunflower seed shell for high CO₂ adsorption. *Adsorption* **2015**, *21*, 125–133. [CrossRef]
15. Plaza, M.G.; Gonzalez, A.S.; Pevida, C.; Pis, J.J.; Rubiera, F. Valorisation of spent coffee grounds as CO₂ adsorbents for postcombustion capture applications. *Appl. Energy* **2012**, *99*, 272–279. [CrossRef]
16. Wei, H.; Deng, S.; Hu, B.; Chen, Z.; Wang, B.; Huang, J.; Yu, G. Granular bamboo-derived activated carbon for high CO₂ adsorption: The dominant role of narrow micropores. *ChemSusChem* **2012**, *5*, 2354–2360. [CrossRef]
17. Sha, Y.; Lou, J.; Bai, S.; Wu, D.; Liu, B.; Ling, Y. Facile preparation of nitrogen-doped porous carbon from waste tobacco by a simple pre-treatment process and their application in electrochemical capacitor and CO₂ capture. *Mater. Res. Bull.* **2015**, *64*, 327–332. [CrossRef]
18. Heidari, A.; Younesi, H.; Rashidi, A.; Ghoreyshi, A.A. Evaluation of CO₂ adsorption with eucalyptus wood based activated carbon modified by ammonia solution through heat treatment. *Chem. Eng. J.* **2014**, *254*, 503–513. [CrossRef]
19. Department of Statistics Malaysia. Press Release Monthly rubber statistics Malaysia, January 2020. Available online: <https://www.dosm.gov> (accessed on 13 March 2020).
20. Tran, H.N.; You, S.-J.; Chao, H.-P. Fast and efficient adsorption of methylene green 5 on activated carbon prepared from new chemical activation method. *J. Environ. Manag.* **2017**, *188*, 322–336. [CrossRef]
21. Houshmand, A.; Wan Daud, W.M.A.; Shafeeyan, M.S. Exploring potential methods for anchoring amine groups on the surface of activated carbon for CO₂ adsorption. *Sep. Sci. Technol.* **2011**, *46*, 1098–1112. [CrossRef]
22. Plaza, M.G.; Pevida, C.; Arenillas, A.; Rubiera, F.; Pis, J.J. CO₂ capture by adsorption with nitrogen enriched carbons. *Fuel* **2007**, *86*, 2204–2212. [CrossRef]
23. Arenillas, A.; Smith, K.M.; Drage, T.C.; Snape, C.E. CO₂ capture using some fly ash-derived carbon materials. *Fuel* **2005**, *84*, 2204–2210. [CrossRef]
24. Maroto-Valer, M.M.; Lu, Z.; Zhang, Y.; Tang, Z. Sorbents for CO₂ capture from high carbon fly ashes. *Waste Manag.* **2008**, *28*, 2320–2328. [CrossRef]
25. Wei, J.; Shi, J.; Pan, H.; Zhao, W.; Ye, Q.; Shi, Y. Adsorption of carbon dioxide on organically functionalized SBA-16. *Microporous Mesoporous Mater.* **2008**, *116*, 394–399. [CrossRef]
26. He, X.; Zhu, J.; Wang, H.; Zhou, M.; Zhang, S. Surface functionalization of activated carbon with phosphonium ionic liquid for CO₂ adsorption. *Coatings* **2019**, *9*, 590. [CrossRef]
27. Girish, C.R. Various impregnation methods used for the surface modification of the adsorbent: A review. *Int. J. Eng. Technol.* **2018**, *7*, 330–334. [CrossRef]
28. Jain, S.; Bansiwala, A.; Biniwale, R.B.; Milmile, S.; Das, S.; Tiwari, S.; Antony, P.S. Enhancing adsorption of nitrate using metal impregnated alumina. *J. Environ. Chem. Eng.* **2015**, *3*, 232–2349. [CrossRef]

29. Zhu, J.; He, B.; Huang, J.; Li, C.; Ren, T. Effect of immobilization methods and the pore structure on CO₂ separation performance in silica-supported ionic liquids. *Microporous Mesoporous Mater.* **2018**, *260*, 190–200. [[CrossRef](#)]
30. Sanz-Perez, E.S.; Arencibia, A.; Calleja, G.; Sanz, R. Tuning the textural properties of HMS mesoporous silica. Functionalization towards CO₂ adsorption. *Microporous Mesoporous Mater.* **2018**, *260*, 235–244. [[CrossRef](#)]
31. Houshmand, A.; Wan Daud, W.M.A.; Lee, M.-G.; Shafeeyan, M.S. Carbon dioxide capture with amine-grafted activated carbon. *Water Air Soil Pollut.* **2012**, *223*, 827–835. [[CrossRef](#)]
32. Maroto-Valer, M.M.; Tang, Z.; Zhang, Y. CO₂ capture by activated and impregnated anthracites. *Fuel Process. Technol.* **2005**, *86*, 1487–1502. [[CrossRef](#)]
33. Bezerra, D.P.; Oliveira, R.S.; Vieira, R.S.; Cavalcante, C.L., Jr. Adsorption of CO₂ on nitrogen-enriched activated carbon and zeolite 13X. *Adsorption* **2011**, *17*, 235–246. [[CrossRef](#)]
34. Aroua, M.K.; Wan Daud, W.M.A.; Yin, C.Y.; Adinata, D. Adsorption capacities of carbon dioxide, oxygen, nitrogen and methane on carbon molecular basket derived from polyethyleneimine impregnation on microporous palm shell activated carbon. *Sep. Purif. Technol.* **2008**, *62*, 609–613. [[CrossRef](#)]
35. Zhang, C.; Song, W.; Sun, G.; Xie, L.; Wang, J.; Li, K.; Sun, C.; Liu, H.; Snape, C.E.; Drage, T. CO₂ capture with activated carbon grafted by nitrogenous functional groups. *Energy Fuels* **2013**, *27*, 4818–4823. [[CrossRef](#)]
36. Grondein, A.; Bélanger, D. Chemical modification of carbon powders with aminophenyl and aryl-aliphatic amine groups by reduction of in situ generated diazonium cations: Applicability of the grafted powder towards CO₂ capture. *Fuel* **2011**, *90*, 2684–2693. [[CrossRef](#)]
37. McDonald, J.D.; Kracko, D.; Doyle-Eisele, M.; Garner, C.E.; Wegerski, C.; Senft, A.; Knipping, E.; Shaw, S.; Rohr, A. Carbon capture and sequestration: An exploratory inhalation toxicity assessment of amine-trapping solvents and their degradation products. *Environ. Sci. Technol.* **2014**, *48*, 10821–10828. [[CrossRef](#)]
38. Ahmed, S.; Ramli, A.; Yusup, S. Development of polyethylenimine-functionalized mesoporous Si-MCM-41 for CO₂ adsorption. *Fuel Process. Technol.* **2017**, *167*, 622–630. [[CrossRef](#)]
39. Xu, X.; Song, C.; Andresen, J.M.; Miller, B.G.; Scaroni, A.W. Novel polyethylenimine-modified mesoporous molecular sieve of MCM-41 type as high-capacity adsorbent for CO₂ capture. *Energy Fuels* **2002**, *16*, 1463–1469. [[CrossRef](#)]
40. Franchi, R.S.; Harlick, P.J.E.; Sayari, A. Applications of pore-expanded mesoporous silica. 2. Development of a high-capacity, water-tolerant adsorbent for CO₂. *Ind. Eng. Chem. Res.* **2005**, *44*, 8007–8013. [[CrossRef](#)]
41. Hasib-ur-Rahman, M.; Siaj, M.; Larachi, F. Ionic liquids for CO₂ capture-Development and progress. *Chem. Eng. Process.* **2010**, *49*, 313–322. [[CrossRef](#)]
42. Lemus, J.; Palomar, J.; Gilarranz, M.A.; Rodriguez, J.J. Characterization of supported ionic liquid phase (SILP) materials prepared from different supports. *Adsorption* **2011**, *17*, 561–571. [[CrossRef](#)]
43. Ban, Y.; Li, Z.; Li, P.D.Y.; Peng, Y.; Jin, H.; Wenmei, J.; Guo, A.; Wang, P.; Yang, P.D.Q.; Zhong, P.D.C.; et al. Confinement of ionic liquids in nanocages: Tailoring the molecular sieving properties of ZIF-8 for membrane based CO₂ capture. *Angew. Chem.* **2015**, *54*, 15483–15487. [[CrossRef](#)] [[PubMed](#)]
44. Yusuf, N.Y.; Masdar, M.S.; Isahak, W.N.R.W.; Nordin, D.; Husaini, T.; Majlan, E.H.; Rejab, S.A.M.; Chew, C.L. Ionic-liquid impregnated activated carbon for biohydrogen purification in an adsorption unit. In Proceedings of the IOP Conference Series: Materials Science and Engineering, 29th Symposium of Malaysian Chemical Engineers (SOMChE) 2016, Miri, Sarawak, Malaysia, 1–3 December 2016; IOP Publishing Ltd.: Bristol, UK, 2017.
45. Aki, S.N.V.K.; Mellein, B.R.; Saurer, E.M.; Brennecke, J.F. High pressure phase behavior of carbon dioxide with imidazolium-based ionic liquids. *J. Phys. Chem. B* **2004**, *108*, 20355–20365. [[CrossRef](#)]
46. Ramdin, M.; de Loos, T.W.; Vlucht, T.J.H. State-of-the-art of CO₂ capture with ionic liquids. *Ind. Eng. Chem. Res.* **2012**, *51*, 8149–8177. [[CrossRef](#)]
47. Blanchard, L.A.; Hancu, D.; Beckman, E.J.; Brennecke, J.F. Green processing using ionic liquids and CO₂. *Nature* **1999**, *399*, 28–29. [[CrossRef](#)]
48. Revelli, A.-L.; Mutelet, F.; Jaubert, J.N. High carbon dioxide solubilities in imidazolium-based ionic liquids and in poly(ethylene glycol) Dimethyl ether. *J. Phys. Chem. B* **2010**, *114*, 12908–12913. [[CrossRef](#)]
49. Cadena, C.; Anthony, J.L.; Shah, J.K.; Morrow, T.I.; Brennecke, J.F.; Maginn, E.J. Why is CO₂ so soluble in imidazolium-based ionic liquids? *J. Am. Chem. Soc.* **2004**, *126*, 5300–5308. [[CrossRef](#)]
50. Jung, Y.-H.; Jung, J.-Y.; Jin, Y.-R.; Lee, B.-C.; Baek, I.-H.; Kim, S.-H. Solubility of carbon dioxide in imidazolium-based ionic liquids with a methanesulfonate anion. *J. Chem. Eng. Data* **2012**, *57*, 3321–3329. [[CrossRef](#)]
51. Kumelan, J.; Tuma, D.; Kamps, A.P.-S.; Maurer, G. Solubility of the single gases carbon dioxide and hydrogen in the ionic liquid [bmpy][Tf₂N]. *J. Chem. Eng. Data* **2010**, *55*, 165–172. [[CrossRef](#)]
52. Zhang, Y.; Xing, W.; Liu, S.; Liu, Y.; Yang, M.; Zhao, J.; Song, Y. Pure methane, carbon dioxide, and nitrogen adsorption on anthracite from china over a wide range of pressures and temperatures: Experiments and modeling. *RSC Adv.* **2015**, *5*, 52612–52623. [[CrossRef](#)]
53. Erto, A.; Silvestre-Alberio, A.; Silvestre-Alberio, J.; Rodriguez-Reinoso, F.; Balsamo, M.; Lancia, A.; Fabio, M. Carbon-supported ionic liquids as innovative adsorbents for CO₂ separation from synthetic flue-gas. *J. Colloid Interface Sci.* **2015**, *448*, 41–50. [[CrossRef](#)]

54. Singh, K.S.W.; Everett, D.H.; Haul, R.A.W.; Moscou, L.; Pierotti, R.A.; Rouquerol, J.; Siemieniowska, T. Reporting physisorption data for gas/solid systems with special reference to the determination of surface area and porosity (recommendations 1984). *Pure Appl. Chem.* **1985**, *57*, 603–619. [[CrossRef](#)]
55. Esteves, I.A.A.C.; Lopes, M.S.S.; Nunes, P.M.C.; Mota, J.P.B. Adsorption of natural gas and biogas components on activated carbon. *Sep. Purif. Technol.* **2008**, *62*, 281–296. [[CrossRef](#)]
56. Ammendola, P.; Raganati, F.; Chirone, R. CO₂ adsorption on a fine activated carbon in a sound assisted fluidized bed: Thermodynamics and kinetics. *Chem. Eng. J.* **2017**, *322*, 302–313. [[CrossRef](#)]
57. Tamilarasan, P.; Ramaprabhu, S. Polyaniline-magnetite nanocapsules based nanocomposite for carbon dioxide adsorption. *Int. J. Greenh. Gas Control.* **2012**, *10*, 486–493. [[CrossRef](#)]
58. Zhang, W.; Gao, E.; Li, Y.; Bernards, M.T.; He, Y.; Shi, Y. CO₂ capture with polyamine-based protic ionic liquid functionalized mesoporous silica. *J. CO₂ Util.* **2019**, *34*, 606–615. [[CrossRef](#)]
59. Boonpoke, A.; Chiarakorn, S.; Laosiripojana, N.; Towprayoon, S. Synthesis of activated carbon and MCM-41 from bagasse and rice husk and their carbon dioxide adsorption. *J. Sustain. Energy Environ.* **2011**, *2*, 77–81.
60. Nasri, N.S.; Hamza, U.D.; Ismail, S.N.; Ahmed, M.M.; Mohsin, R. Assessment of porous carbons derived from sustainable palm solid waste for carbon dioxide capture. *J. Clean. Prod.* **2014**, *71*, 148–157. [[CrossRef](#)]
61. Xu, Q.-Q.; Yin, J.-Z.; Zhou, X.-L.; Yin, G.-Z.; Liu, Y.-F.; Cai, P.; Wang, A.-Q. Impregnation of ionic liquids in mesoporous silica using supercritical carbon dioxide and co-solvent. *RSC Adv.* **2016**, *6*, 101079–101086. [[CrossRef](#)]
62. Yin, J.-Z.; Zhen, M.-Y.; Cai, P.; Zhou, D.; Li, Z.-J.; Zhu, H.-Y.; Xu, Q.-Q. Supercritical CO₂ preparation of SBA-15 supported ionic liquid and its adsorption for CO₂. *Mater. Res. Express* **2018**, *5*, 065060. [[CrossRef](#)]
63. Marliza, T.S.; Yarmo, M.A.; Hakim, A.; Abu Tahari, M.N.; Hisham, M.W.M.; Taufiq-Yap, Y.H. CO₂ capture on NiO supported imidazolium-based ionic liquid. In Proceedings of the AIP Conference Proceedings, 2017, Selangor, Malaysia, 28–30 November 2016.
64. Aquino, A.S.; Bernard, F.L.; Borges, J.V.; Mafra, L.; Vecchia, F.D.; Vieira, M.O.; Ligabue, R.; Seferin, M.; Chaban, V.V.; Cabrita, E.J.; et al. Rationalizing the role of the anion in CO₂ capture and conversion using imidazolium based ionic liquid modified mesoporous silica. *RSC Adv.* **2015**, *5*, 64220–64227. [[CrossRef](#)]